2001

Automatic 3D Registration of Lung Surfaces in Computed Tomography Scans

Automatic 3D Registration of Lung Surfaces in Computed Tomography Scans

Margrit Betke, PhD[1], Harrison Hong, BA[1], and Jane P. Ko, MD[2]

[1] Computer Science Department
Boston University,
Boston, MA 02215, USA
betke@cs.bu.edu
http://www.cs.bu.edu/faculty/betke

[2] Department of Radiology
New York University Medical School
New York, NY 10016, USA

Abstract. We developed an automated system that registers chest CT scans temporally. Our registration method matches corresponding anatomical landmarks to obtain initial registration parameters. The initial point-to-point registration is then generalized to an iterative surface-to-surface registration method. Our "goodness-of-fit" measure is evaluated at each step in the iterative scheme until the registration performance is sufficient. We applied our method to register the 3D lung surfaces of 11 pairs of chest CT scans and report promising registration performance.[1]

1 Introduction

Chest computed tomography (CT) has become a well-established means of diagnosing primary lung cancer and pulmonary metastases and evaluating response of these malignant lesions to treatments. Diagnosis and prognosis of cancer generally depend upon growth assessment of pulmonary lesions on repeat CT studies [44, 29]. Chest CT scans can also be used for lung cancer screening, which has been proposed by some but is still controversial. Bronchogenic cancer remains the leading cause of cancer death in the United States, killing 160,000 people a year. The overall 5-year survival rate is now 15% [20], but early detection and resection can improve the prognosis significantly. For example, the 5-year survival rate for Stage I cancer is 67% [28].

Our long-term objective is to develop an image analysis system that supports the radiologist in detecting and comparing pulmonary nodules in repeated CT studies in a clinical setting. Such a system must solve the classical problems in medical image analysis – segmentation, detection, and registration – for the important domain of chest CT images. References [5] and [19] describe our preliminary system that automatically segments the thorax, lungs, and structures

[1] The support of the Office of Naval Research, National Science Foundation, and Radiological Society of North America is gratefully acknowledged.

within the lungs, and detects nodules in axial chest CT images. In this system, human intervention is needed to register the CT studies. In the current paper, we focus on automating the registration task and introduce a method for automatic three-dimensional (3D) alignment of lung surfaces in repeat CT scans.

A large body of literature has been published on registration techniques. References [8] and [40] provide excellent surveys. Registration methods in the medical image domain focus primarily on the brain, e.g., [1, 9, 10, 12, 14, 21–23, 39, 41, 46], but also other organ systems, such as spine [13, 31], foot [34], breast [36, 43], and prostate [3].

Registration of images within the same modality, e.g., CT with CT or magnetic resonance (MR) with MR, and across modalities has been addressed. CT images have been correlated with MR images [22, 23, 33, 35] and positron emission tomography (PET) with MR images [18, 23, 30, 32, 33, 37, 38] for the brain. MR and CT scans of the head have been registered to the patient skin surface depth data obtained by a laser range scanner [12]. Bone scans have been registered with bone films [34] for the foot. CT studies of the thorax have been registered to PET studies [45] and bronchoscopic images [7].

Some registration approaches ensure that data sets are obtained with prospective attention to patient positioning, for example, through head fixation; others retrospectively reorient image sets using fixed external skin-surface or bone-implanted fiducial markers [11, 24, 26]. Techniques have been developed to register points to points [16] or surfaces [4, 25, 26, 30], and correlate subimages [2, 17, 42]. Often only a small misalignment of the images is assumed [2]. Other registration methods require some manual input to compensate for rotational and translational differences between two studies [18, 30].

Registration of chest radiographs has been addressed by Kano et al. [17]. To the best of our knowledge, an automated system to register chest CT images temporally has not been developed yet. Registration of thoracic CT studies is challenging, since patient position and orientation varies each time a study is obtained. Other obstacles are differences in inspiratory volumes. The patient's thorax is imaged when the patient is in maximal inspiration for the entire scan. Not all patients, however, can comply with this request.

In this paper, the lung surfaces of two CT scans are segmented and registered for 11 patients. The scans were taken solely for clinical reasons and without external fiducial markers or any particular attention to patient position. We first describe an anatomical landmark-based registration method in Sections 2.1 – 2.3. We then generalize it to surface-to-surface registration in Section 2.4. In Section 2.5, we improve the method using an iterative registration algorithm that is based a registration scheme by Besl [4]. We then report registration results for 11 pairs of chest CT scans in Section 3 and conclude with a discussion in Section 4.

2 Methods

Registration techniques relate points in two different data sets to each other. The geometric nature of a registration transformation can be described by its "elasticity" [40]. The degree of elasticity increases from rigid to affine to curved mappings. Rigid-body transformations describe translations and rotations within the image plane. Affine transformations map straight lines to straight lines and therefore allow scaling and skewing of the data in addition to rotation and translation. Curved transformations map straight lines into curves, for example with polynomial mappings or other deformations.

In this section, we first describe a registration method for anatomical landmarks that is based on an affine point-to-point transformation that models 3D rotation and translation, as well as scaling. We then generalize the affine transformation to curve-to-curve and surface-to-surface registration and finally propose an iterative scheme to improve the surface-to-surface registration.

2.1 Registration of Anatomical Landmarks

Registration techniques determine the *absolute orientation* of one data set with respect to the other. When used in the computer vision or photogrammetry literature, the term "absolute orientation" generally implies that the 3D coordinates of corresponding points in the two different data sets are known [15]. For our 3D data sets, it is difficult to establish the anatomical correspondence of most voxels, even for a human observer. We therefore use the voxels that make up anatomical landmarks, such as spine and sternum, for our initial registration method. Note that we do not use external fiduciary markers, since they would be impractical in a clinical setting.

Bones are rigid anatomical features that can be registered reliably with a 3D affine transformation that models rotation, translation, and scaling. In particular, the sternum and vertebrae are excellent anatomical landmarks, because their positions are relatively fixed within the chest. We estimate the 3D position of anatomical landmarks by identifying the landmarks in the axial images and calculating their centroids.

We also use the trachea as an anatomical landmark. Although trachea position and shape change with respiration, we found that the tracheal centroids in the axial images serve as reliable landmarks for registration of our data sets. Finally, we also tested the use of structures within the lungs, for example nodules, for registration. Figure 1 shows how the centroids of sternum, trachea, and a nodule in the left lung are registered in corresponding axial images of two CT data sets.

We describe a method to detect anatomical landmarks in Section 2.2 and the 3D affine landmark-to-landmark transformation in Section 2.3.

2.2 Correlation-Based Recognition of Anatomical Features.

We use template images of anatomical landmarks, for example, sternum, vertebra, and trachea, as shown in Fig. 1, to detect these landmarks in our test data.

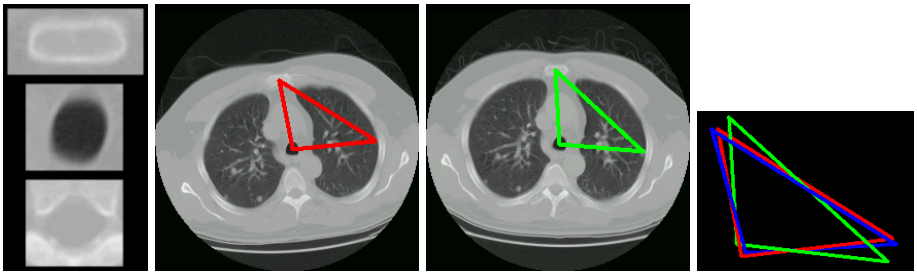

Fig. 1. On the left, template images of the sternum, trachea, and spine are shown. In the middle, two corresponding CT images are shown that are part of two different CT studies of the same patient. The landmarks chosen for the initial registration are the centroids of the sternum, trachea, and a nodule in the left lung. The green test points in study 2 must be matched to the red model points in study 1. On the right, the best affine transformation of the green test points is shown in blue.

The template images are created offline by manually cropping subimages of the features out of a training data set. Although the features look slightly different in the test data, training and test data generally match well. This is particularly true if we use a deformable template that can be scaled or rotated.

Let $\mathbf{a}$ describe the affine parameters position, scale, and rotation of the template. We use the normalized correlation coefficient to find the best estimate of the affine parameters. In our previous work [6], we showed that the statistically optimal estimator for the affine parameters takes the form of the normalized correlation coefficient. It quantifies how well the measured data in subimage $I_q(x, y)$ matches the template feature in $q(x, y; \mathbf{a})$ and serves as a match measure that is "information conserving" because it exploits all the measured data relevant to the feature's recognition. The normalized correlation coefficient is defined by

$$r(\mathbf{a}) \;=\; \frac{1}{\sigma_I(\mathbf{a})\sigma_q(\mathbf{a})}\Big(A(\mathbf{a}) \sum_{(x,y)\in O} I_q(x,y)q(x,y;\mathbf{a}) - m_I(\mathbf{a})m_q(\mathbf{a})\Big), \qquad (1)$$

where $m_I(\mathbf{a}) = \sum I_q(x, y)$ and $m_q(\mathbf{a}) = \sum q(x, y; \mathbf{a})$ are the respective local image means, $\sigma_I^2(\mathbf{a}) = A(\mathbf{a}) \sum I_q(x, y)^2 - \left(\sum I_q(x, y)\right)^2$ and $\sigma_q^2(\mathbf{a}) = A(\mathbf{a}) \sum q(x, y; \mathbf{a})^2 - \left(\sum q(x, y; \mathbf{a})\right)^2$ are the respective local variances, and where the sums are computed over a region O that is the union of all pixels that contain the expected feature and $A = |O|$ is the number of pixels in O.

We propose a hierarchical method of search for the global peak that computes the correlation coefficient at different resolution scales. For position estimation, for example, we choose a grid-based approach which samples the ambiguity surface at every 10th pixel, then around local peaks at every 5th pixel, and then eventually in the surrounding of maximum peak at every pixel. The ambiguity surfaces for the position estimates of anatomical features have global peaks with correlations of at least 0.8, which lie far above the expected correlation $E[r(\mathbf{a})] = 0$. In addition, once a feature, such as the trachea, is found in an axial

image, the search space for the same feature in subsequent images can be reduced significantly. In addition, the template feature q can automatically be updated online with the cropped image of the detected feature in the previous slice. This results in high correlations (above 0.9) and reliable estimates of feature position and size.

2.3 Three-Dimensional Affine Point-to-Point Registration.

Given a voxel $\mathbf{x}$ in study 1 and a voxel $\mathbf{p}$ in study 2, the general 3D affine transformation

$$\mathbf{x} = \mathbf{A}\mathbf{p} + \mathbf{x_0} \tag{2}$$

maps $\mathbf{p}$ into $\mathbf{x}$, where the 3×3 matrix $\mathbf{A}$ can be expressed in terms of nine parameters, three for rotation, three for scaling, and three for skewing. Vector $\mathbf{x_0}$ describes the 3D translation between $\mathbf{x}$ and $\mathbf{p}$.

In our application, the orientation of the patient's body on the CT table is modeled by rotation around the x, y, and z axes. Parameters that model scaling in the x- and y-dimensions are needed if the field-of-view, i.e., the pixel-width-to-millimeter ratio, differs between two studies. Scaling is usually uniform in the x- and y- but not in the z-dimension. Scaling in z is due to the differing slice thickness and number of slices in the two studies. Note that the scaling parameters are determined before scan acquisition. We therefore do not need to invert for the scaling parameters, but instead directly use the field-of-view and collimation information provided with the scan data. We assume that the CT scanner does not introduce skewing and preserves the Cartesian (or rectangular) coordinates of 3D points. Then the problem of finding the general affine transformation between two CT studies reduces to the problem of finding the rigid-body transformation between the two studies after they have been adjusted for scaling differences.
The rigid-body transformation $\mathcal{T}$ maps $\mathbf{p}$ into $\mathbf{x}$,

$$\mathbf{x} = \mathcal{T}(\mathbf{p}) = \mathbf{R}\mathbf{p} + \mathbf{x_0}, \tag{3}$$

where the orthonormal 3×3 matrix $\mathbf{R}$ rotates $\mathbf{p}$ into vector $\mathbf{R}\mathbf{p}$, which is then shifted into $\mathbf{x}$ by translation vector $\mathbf{x_0}$. We have 12 unknowns (9 matrix coefficients and 3 translation parameters) and only 3 linear equations. So we need at least 4 corresponding points to compute the unknown transformation parameters. If we impose the orthonormality condition, we obtain an additional equation and therefore only need 3 corresponding points. Note that these three points must not be collinear.

Since there may be errors in the measurement of the points or in the corresponding landmark detection algorithm, a greater accuracy in determining the transformation parameters can be obtained if more than three points are used. Given a set X of n points $\mathbf{x}_1, \ldots, \mathbf{x}_n$ in study 1 and a set P of corresponding points $\mathbf{p}_1, \ldots, \mathbf{p}_n$ in study 2, our goal is to minimize the sum of square residual errors

$$\sum_{i=1}^{n} \|\mathbf{e}_i\|^2 = \sum_{i=1}^{n} \|\mathbf{x}_i - \mathcal{T}(\mathbf{p}_i)\|^2 = \sum_{i=1}^{n} \|\mathbf{x}_i - \mathbf{R}\mathbf{p}_i - \mathbf{x_0}\|^2 \tag{4}$$

with respect to the unknowns $\mathbf{R}$ and $\mathbf{x_0}$. A closed-form optimal solution to this least-squares problem was given by Horn [16]. The advantages of his solution are that an iterative scheme or initial guess are not required. The best possible transformation is computed in one step. An additional advantage is that the solution is symmetric, which means that the solution that transforms P into X is the exact inverse of the solution that transforms X into P.

The best translation vector $\hat{\mathbf{x}}_\mathbf{0}$ is the difference between the centroid $\bar{\mathbf{x}} = 1/n \sum_{i=1}^{n} \mathbf{x}_i$ of point set X and the centroid $\bar{\mathbf{p}} = 1/n \sum_{i=1}^{n} \mathbf{p}_i$ of point set P rotated by rotation $\mathbf{R}$:

$$\mathbf{x_0} = \bar{\mathbf{x}} - \mathbf{R}(\bar{\mathbf{p}}). \tag{5}$$

Therefore, the translation can be computed easily once the rotation is found. To find the rotation, the coordinates of voxels in X and P are converted into coordinates of voxels in X' and P' of coordinate systems that are originated at the respective centroids, e.g., $\mathbf{x'_i} = \mathbf{x_i} - \bar{\mathbf{x}}$ for all $\mathbf{x_i} \in X$. This reduces the least-squares problem of Eq. 4 to a minimization of

$$\sum_{i=1}^{n} \|\mathbf{x}'_i - \mathbf{R}\mathbf{p}'_i\|^2 = \sum_{i=1}^{n} \|\mathbf{x}'_i\|^2 - 2\sum_{i=1}^{n} \mathbf{x}_i'^T \mathbf{R}\mathbf{p}'_i + \sum_{i=1}^{n} \|\mathbf{p}'_i\|^2 \tag{6}$$

with respect to rotation $\mathbf{R}$ only, or

$$\max_{\mathbf{R}} \sum_{i=1}^{n} \mathbf{x}_i'^T \mathbf{R}\mathbf{p}'_i. \tag{7}$$

The solution of this maximization problem is

$$\mathbf{R} = \begin{pmatrix} q_0^2 + q_x^2 - q_y^2 - q_z^2 & 2(q_x q_y - q_0 q_z) & 2(q_x q_z - q_0 q_y) \\ 2(q_y q_x - q_0 q_z) & q_0^2 - q_x^2 + q_y^2 - q_z^2 & 2(q_y q_z - q_0 q_x) \\ 2(q_z q_x - q_0 q_y) & 2(q_z q_y + q_0 q_x) & q_0^2 - q_x^2 - q_y^2 + q_z^2 \end{pmatrix}, \tag{8}$$

where $q = (q_0, q_x, q_y, q_z)$ is the unit eigenvector that corresponds to the maximum eigenvalue of the symmetric matrix

$$\mathbf{N} = \begin{pmatrix} s_{xx} + s_{yy} + s_{zz} & s_{yz} - s_{zy} & s_{zx} - s_{xz} & s_{xy} - s_{yz} \\ s_{yz} - s_{zy} & s_{xx} - s_{yy} - s_{zz} & s_{xy} + s_{yz} & s_{zx} + s_{xz} \\ s_{zx} - s_{xz} & s_{xy} + s_{yz} & -s_{xx} + s_{yy} - s_{zz} & s_{yz} + s_{zy} \\ s_{xy} - s_{yx} & s_{zx} + s_{xz} & s_{yz} + s_{zy} & -s_{xx} - s_{yy} + s_{zz} \end{pmatrix}, \tag{9}$$

and s_{kl} is the kl-th component of outer-product matrix $\mathbf{S} = \sum_i^n \mathbf{x}'_i \mathbf{p}_i'^T$.

In Figure 1, the centroids of the sternum, trachea, and a nodule in study 1, shown in red, make up the model set $X = \{\mathbf{x}_1, \mathbf{x}_2, \mathbf{x}_3\}$ and the corresponding centroids in study 2, shown in green, make up the test set $P = \{\mathbf{p}_1, \mathbf{p}_2, \mathbf{p}_3\}$. First we compute the rotation matrix using Eq. 8, then the translation parameters using Eq. 5, and finally the transformation $\mathcal{T}$ of P into X using Eq. 3, which is illustrated in blue in Fig. 1. We use Eq. 4 to report the "goodness of fit."

2.4 Three-Dimensional Affine Shape Registration.

In this paper, we focus on the surface of the lung parenchyma that is segmented from the full 3D data set using the method described in our earlier work [19, 5]. Figure 2 demonstrates a 3D view of the lung surface. The lung parenchyma was segmented on each of the axial images of a low-dose chest CT scan. The scan was reconstructed at 1.0 mm intervals and with a 1.25 mm slice thickness. Our algorithm identifies the lung borders of the parenchyma and uses them to construct the 3D surface view of the lung parenchyma. Our goal is to register the lung surfaces segmented on an initial CT scan to the lung surfaces segmented on another CT scan of the same patient obtained at a later time.

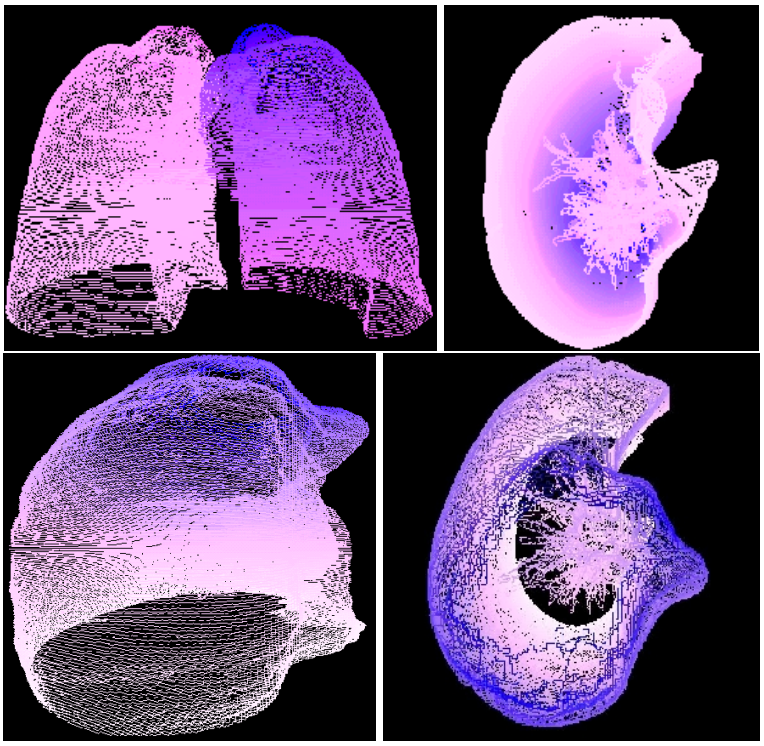

Fig. 2. 3D visualization of the lung. Top left image: coronal view of both lungs. Top right image: top-down axial view of one lung. Bottom images: wire-frame visualization of one lung.

The point-to-point registration algorithm described above provides the absolute orientation of one point set P with respect to the other point set X. It assumes that the correspondence between points $\mathbf{x}_i$ and $\mathbf{p}_i$, for each i, has been established. For certain points, for example the centroids of the sternum in corresponding axial slices, correspondence can be determined with relatively high

confidence, but for other point pairs, their correspondences are not as easily established. For example, a lung border point in the apex of study 1 corresponds to *some* border point in the apex of study 2, but *which* point generally cannot be determined, even by a human observer. This is true for points that are pixels on curves in corresponding 2D axial images, as well as voxels on 3D surfaces. We therefore define the correspondence $\mathcal{C}$ of two points on different curves or surfaces by their distances to each other and the rest of the points. In particular, test point $\mathbf{p}_i$ corresponds to model point $\mathbf{x}_j = \mathcal{C}(\mathbf{p}_i)$, if their Euclidean distance is the shortest among all distances between $\mathbf{p}_i$ and any point in X, i.e.,

$$\mathcal{C}(\mathbf{p}_i) = \mathbf{x}_j \quad \text{for which} \quad \|\mathbf{x}_j - \mathbf{p}_i\| = \min_{\mathbf{x}_k \in X} \|\mathbf{x}_k - \mathbf{p}_i\|. \tag{10}$$

Note that $\mathcal{C}$ is not a symmetric mapping, i.e., the corresponding test point $\mathbf{p}_r = \mathcal{C}(\mathbf{x}_j)$ of model point $\mathbf{x}_j$ is not necessarily $\mathbf{p}_i$, since the shortest distance among all distances between $\mathbf{x}_j$ and any point in P,

$$\min_{\mathbf{p}_s \in P} \|\mathbf{x}_j - \mathbf{p}_s\|, \tag{11}$$

may be shorter than $\|\mathbf{x}_j - \mathbf{p}_i\|$. Using the definition for correspondence in Eq. 10, we can match two curves or two surfaces to each other that contain a different number of pixels or voxels.

The correspondence definition in Eq. 10 is reliable if the two data sets are close to each other, in particular, if they have been registered. This creates a paradoxical situation: we would like to register corresponding points, but need to register them first in order to establish their correspondences. To resolve this situation, we solve the registration and correspondence problems concurrently. We developed an iterative approach based on Besl's iterative closest-point algorithm [4].

We first detect anatomical landmarks in studies 1 and 2 and compute the 3D affine transformation that registers them optimally, as described in Section 2.3. We then segment the lungs [19, 5] and register them with the transformation parameters computed for the landmark registration. We establish correspondences by computing the Euclidean distances between all point pairs of the two data sets. If the registration error is too large, we register the transformed lung borders in study 2 to the lung borders in study 1, compute the new correspondences and registration error, and then iterate. Once the error is sufficiently small, we terminate the process. Convergence of this iterative algorithm can be shown [4]. The pseudo-code of our method is given below.

2.5 Registration Code

Function `LungRegistration` takes as inputs 3D voxel data sets `CTstudy1` and `CTstudy1` that have been adjusted for field-of-view differences, and a parameter `threshold` that is used to decide when the function can terminate with a sufficient registration result. Function `LungRegistration` outputs the transformation parameters for translation and rotation. Its local variables are defined

in lines 2 – 6. For the function calls in lines 7 – 17, we use C-style notation to distinguish input parameters, for example `lung1` in line 14, from parameters that change during the function call, for example `&lungR, &translation,` and `&rotation` in line 14.

```
 1 Function LungRegistration (CTstudy1, CTstudy2, threshold) {
 2   float        error;
 3   voxelset     lung1, lung2, lungR;
 4   voxelset     landmarks1, landmarks2;
 5   voxel        translation;
 6   3x3matrix    rotation;
 7   DetectLandmarks(&landmarks1, &landmarks2);
 8   RegisterLandmarks(landmarks1, landmarks2,
                       &translation, &rotation);
 9   SegmentLungs(CTstudy1, &lung1);
10   SegmentLungs(CTstudy2, &lung2);
11   RegisterLungsInitially(lung1, lung2,
                            translation, rotation, &lungR);
12   ComputeCorrespondencesAndError(lung1, lungR, &error);
13   while (error > threshold) {
14       RegisterLungs(lung1, &lungR, &translation, &rotation);
15       ComputeCorrespondencesAndError(lung1, lungR, &error);
16   }
17   OutputResults(translation, rotation);
18 }
```

Variables `lung1` and `lung2` can either contain the voxels that make up the right and left lungs in the respective CT studies, which means that both lungs will be registered together, or they can contain the voxels of only the right or the left lungs. In the second case, `LungRegistration` must be called twice, once for the right, and once for the left lung registration. Figure 3 shows the results of joint and separate lung registrations for the 2D case, Fig. 4 the results of registering 3D data sets that contain ten left lung contours, and Fig. 5 the results of registering the full 3D lung surfaces of a right lung. Visual inspection shows that the red measured and blue computed points match well and confirms the quantitative error analysis.

3 Results

Eleven patients with cancer diagnoses and pulmonary nodules were selected, who had thoracic CT scans for clinical indications between April 1993 and August 2000. The selected patients each had two CT studies, and a total of 22 CT studies was evaluated. Ten chest CT scans had been performed helically on GE HiSpeed Advantage machines (GE Medical Systems, Milwaukee, WI) according to the standard departmental protocol. The scans were obtained from the lung apices through the adrenal glands using a 1:1 pitch either with $5mm$ collimation for the

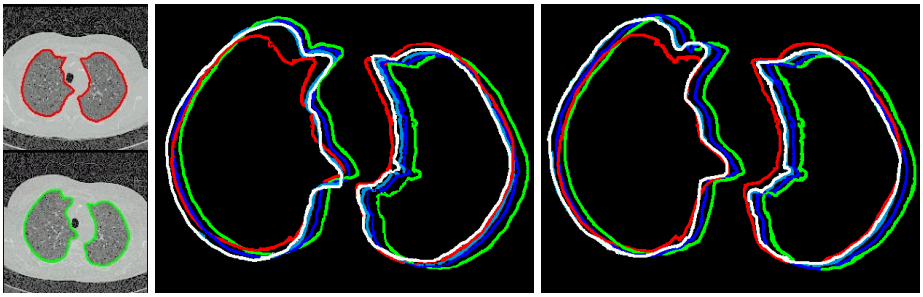

Fig. 3. Visualization of 2D lung border registration. On the left, two corresponding CT slices are shown with their automatically segmented lung contours in red for study 1 and green for study 2. Three, non-consecutive iterations during the registration process are illustrated in the middle and right images. The green lung borders are first transformed to the dark blue contours, then from there to the light blue contours, and finally, after a few more iterations, to the white contours. In the middle image, the resulting contours are shown when both left and right lungs are registered together. In the right image, the resulting contours are obtained from two registration processes, one for the left lung and one for the right. Note that in both cases, red and white contours match well.

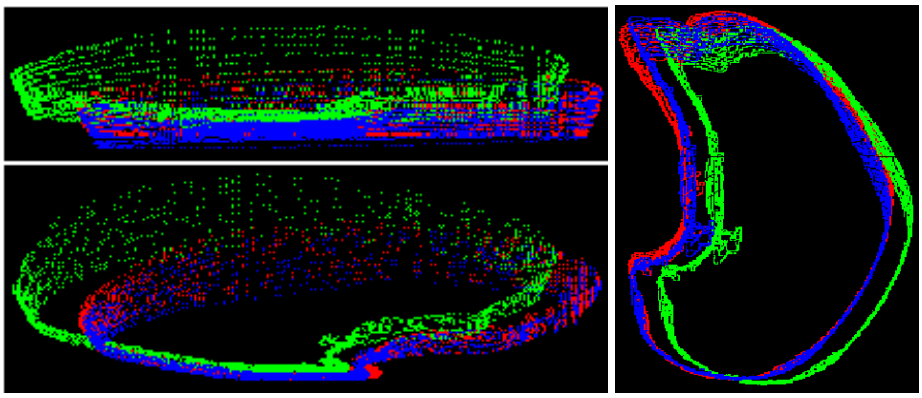

Fig. 4. Visualization of the 3D registration of ten left lung border curves with views from the lung's side (shown in the image on the top left), bottom (bottom left image), and top (right image). The green test points in study 2 are registered to the red model points in study 1 using the transformation that maps green points to blue points. The registration error is minimal.

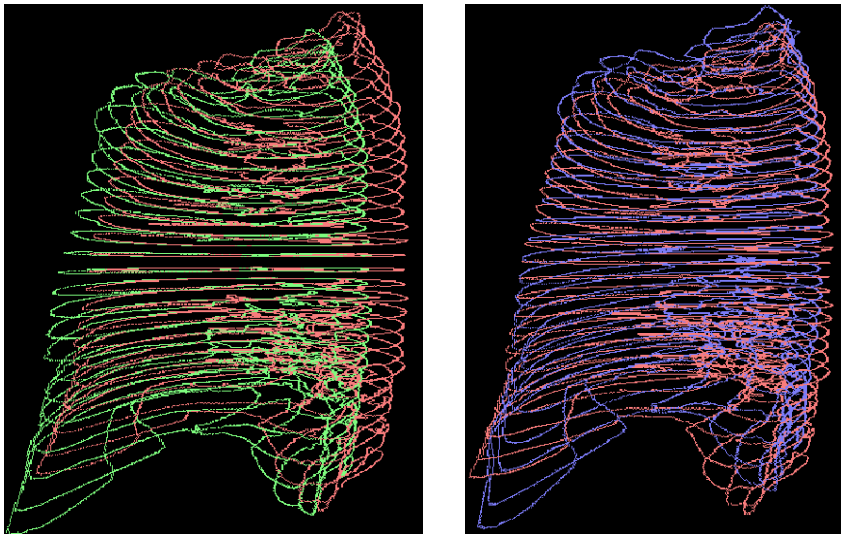

Fig. 5. On the left, wire models of the right lung for study 1 are shown in red and study 2 in green. On the right, the transformed lung surface of study 2 is shown in blue. It matches well with the lung surface of study 1, shown again in red.

entire study or $10mm$ collimation with $5mm$ collimation through the hila. One study was taken on a multi-helical Somatom Volume Zoom CT (Siemens Medical Systems, Iselin, NJ). The scan was performed using a 1.0 mm collimator and reconstructed in 1.25 mm increments at 1.0 mm intervals. Table 1 summarizes the results.

3.1 Registration Speed

The advantage of the initial landmark registration is that it significantly increases the speed of the iterative registration process. Note that we could have merely guessed an initial transformation by leaving out lines 7 and 8 and switching lines 11 and 12 in our pseudo-code. However, depending on the size of the data sets, registration of the full 3D lung surfaces without initial landmark registration takes in the order of hours on a PC with a 866 MHz Pentium III processor. Instead of iterating until the registration error falls below a certain threshold, we fixed the number of iterations to be 25. Figure 6 shows how the error decreases as a function of iteration index. For one of our data sets, after 25 iterations, the registration error reduced to 25% of the initial error. For a data set reconstructed at 5/10/5 mm thickness creating about 2×35 lung slices, 25 iterations take about 2 hours on average. For the data set with 1.25 mm thickness creating about 2×200 lung slices, processing 25 iterations took more than 3 days.

Using initial landmark registration, a much smaller number of iterations is needed to produce sufficient registration results. Including landmark detection

Table 1: Registration Results

Patient	Months between Studies	Reconstruction intervals in mm	No. Lung Slices in Studies 1,2	Ratio of Surface Pts. Studies 2/1	Rotation in Euler Angles (degrees)	Translation in cm
1	2	5/10/5	31 31	89%	(0.4, 0.0, 6.3)	2.9
2	$1\frac{1}{2}$	5	46 53	114%	(1.9, -0.1, 3.9)	3.3
3	4	1	196 202	94%	(1.0, -4.7, -0.5)	1.6
4	74	10/5/10, 5	27 42	154%	(0.5,-0.9, -9.0)	2.6
5	2	5	42 49	115%	(0.2, 0.4, -10.3)	4.0
6	4	10/5/10	29 30	88%	(-0.4, 1.5, -2.1)	1.6
7	$3\frac{1}{2}$	10/5/10	29 30	91%	(0.4, 0.9, -6.3)	6.0
8	1	5	30 29	92%	(-1.5, -1.2, -2.9)	3.7
9	$4\frac{1}{2}$	10/5/10	58 54	98%	(-0.5, 1.5, -6.8)	1.9
10	2	5	43 45	105%	(-2.4, -4.8, 12.8)	9.5
11	$1\frac{1}{4}$	5	48 54	78%	(-1.0, 1.6, -12.2)	7.2

and registration, therefore makes our algorithm more practical and cuts the processing time significantly.

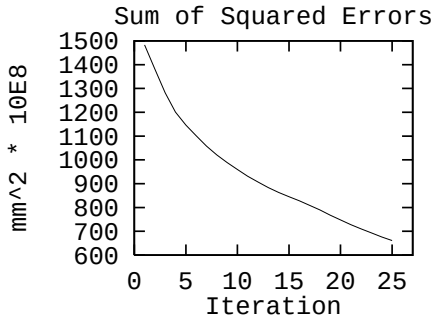

Fig. 6. The sum of squared errors is shown as a function of iteration index for registration of the lung surfaces of patient 2. The error is reported in units of 10^8 mm^2.

4 Discussion and Conclusions

In our preliminary system [19, 5], image-to-image registration required that the lung apices were identified manually on the two studies. Human intervention was also needed to correlate studies with different collimation. To overcome the need of manual intervention, we developed an automatic 3D registration method that matches the lung surfaces in repeated CT studies.

Our lung registration results for the 11 pairs of CT scans are very promising. The performance or "goodness-of-fit" of our registration method is evaluated quantitatively by the sum-of-squared-differences measure and qualitatively by visual inspection. In the future, we will also test whether our system can reliably register corresponding nodules in repeated chest CT scans and thus become a clinically useful tool for nodule growth assessment.

We presented a *global* registration method, which means that any change in a transformation parameter influences the transformation of the 3D data set as a whole [40]. In a *local* transformation, such a change influences only a subset of the data. In the future, we will design deformable models [27] for lung surfaces in order to model local transformations that are due to differences in patient respiration. We will use the deformable model parameters that register lung border surfaces to address the difficult task of registering structures within the lung. This will require modeling the deformable shapes of nodules in 3D and also modeling nodule position as a function of lung surface deformation, since nodules may move within the lung due to the patient's respiration.

Landmark detection and registration significantly improve the speed of the registration process. Since there is a tradeoff between speed and precision of registration, we will test the impact of resolution reduction on registration performance, in particular, nodule registration. We will also investigate whether initial registration of a larger set of landmarks will improve registration precision and speed.

In summary, we have developed a 3D method for registration of lung surfaces in repeated chest CT scans and applied our method to register the lungs scans of 11 patients.

References

1. W. S. I. Ali and F. S. Cohen. Registering coronal histological 2-D sections of a rat brain with coronal sections of a 3-D brain atlas using geometric curve invariants and B-spline representation. *IEEE Trans Med Imag*, 6(17):957–966, 1998.
2. R. J. Althof, M. G. J. Wind, and J. T. Dobbins III. A rapid and automatic image registration algorithm with subpixel accuracy. *IEEE Trans Med Imag*, 16(3):308–316, 1997.
3. R. Bansal, L. Staib, Z. Chen, A. Rangarajan, J. Knisely, R. Nath, and J. Duncan. Entropy-based, multiple-portal-to-3DCT registration for prostate radiotherapy using iteratively estimated segmentation. In C. Taylor and A. Colchester, editors, *Medical Image Computing and Computer-Assisted Intervention – MICCAI'99*, pages 567–578. Springer Verlag, Berlin, 1999.
4. P. J. Besl and N. D. McKay. A method for registration of 3-D shapes. *IEEE Trans Pattern Anal Mach Intell*, 14(2):239–256, 1992.
5. M. Betke and J. P. Ko. Detection of pulmonary nodules on CT and volumetric assessment of change over time. In *Medical Image Computing and Computer-Assisted Intervention – MICCAI'99*, pages 245–252. Springer-Verlag, Berlin, 1999.
6. M. Betke and N. C. Makris. Recognition, resolution and complexity of objects subject to affine transformation. *Int J Comput Vis*, 2001. In press.

7. I. Bricault, G. Ferretti, and P. Cinquin. Registration of real and CT-derived virtual bronchoscopic images to assist transbronchial biopsy. *IEEE Trans Med Imag*, 17(5):703–714, 1998.
8. L. G. Brown. A survey of image registration techniques. *ACM Computing Surveys*, 24(4):325–375, December 1992.
9. M. Chen, T. Kanade, H. A. Rowley, and D. Pomerleau. Anomaly detection through registration. In *Proceedings of the IEEE Computer Vision and Pattern Recognition Conference*, pages 304–310, Santa Barbara, CA, 1998. IEEE Computer Society.
10. C. Davatzikos, J. L. Prince, and R. N. Bryan. Image registration based on boundary mapping. *IEEE Trans Med Imag*, 15(1):112–115, 1996.
11. W. R. Fright and A. D. Linney. Registration of 3-D head surfaces using multiple landmarks. *IEEE Trans Med Imag*, 12(3):515–520, 1993.
12. W.E.L. Grimson, G. J. Ettinger, S. J. White, T. Lozano-Pérez, W. M. Wells III, and R. Kikinis. An automatic registration method for frameless stereotaxy, image guided surgery, and enhanced reality visualization. *IEEE Trans Med Imag*, 15(2):129–140, 1996.
13. J. L. Herring, B. M. Dawant, C. R. Maurer, D. M. Muratore, R. L Galloway, and J. M. Fitzpatrick. Surface-based registration of CT images to phyical space for image-guided surgery of the spine: A sensitivity study. *IEEE Trans Med Imag*, 17(5):743–752, 1998.
14. M. Holden, D. L. G. Hill, E. R. E. Denton, J. M. Jarosz, T. C. S. Cox, T. Rohlfing, J. Goodey, and D. J. Hawkes. Voxel similarity measures for 3-D serial MR brain image registration. *IEEE Trans Med Imag*, 19(2):94–102, 2000.
15. B. K. P. Horn. *Robot Vision*. The MIT Press, Cambridge, MA, 1986.
16. B. K. P. Horn. Closed-form solution of absolute orientation using unit quaternions. *J Opt Soc Am*, 4(4):629–642, 1987.
17. A. Kano, K. Doi, H. MacMahon, D. D. Hassell, and M. L. Giger. Digital image subtraction of temporally sequential chest imagers for detection of interval change. *Med Phys*, 21(3):453–461, 1994.
18. I. Kapouleas, A. Alavi, W. M. Alves, R. E. Gur, and D. W. Weiss. Registration of three-dimensional MR and PET images of the human brain without markers. *Radiology*, 181:731–739, 1991.
19. J. P. Ko and M. Betke. Chest CT: Automated nodule detection and assessment of change over time-preliminary experience. *Radiology*, 218(1):267–273, 2001.
20. S. H. Landis, T. Murray, S. Bolden, and P. A. Wingo. Cancer statistics, 1999. *CA Cancer J Clin*, 49(1):8–31, Jan-Feb 1999.
21. M. E. Leventon and W. E. L. Grimson. Multi-modal volume registration using joint intensity distributions. In W. Wells, A. Colchester, and S. Delp, editors, *Medical Image Computing and Computer-Assisted Intervention – MICCAI'98*, pages 1057–1066. Springer Verlag, Berlin, 1998.
22. A. M. López, D. Lloret, and J. Serrat. Creaseness measures for CT and MR image registration. In *Proceedings of the IEEE Computer Vision and Pattern Recognition Conference*, pages 694–699, Santa Barbara, CA, 1998. IEEE Computer Society.
23. F. Maes, A. Collington, D. Vandermeulen, G. Marchal, and P. Suetens. Multimodality image registration by mutual information. *IEEE Trans Med Imag*, 16(2):187–198, 1997.
24. R. T. Malison, E. G. Miller, R. Greene, G. McCarthy, D. S. Charney, and R. B. Innis. Computer-assisted coregistration of multislice SPECT and MR brain images by fixed external fiducials. *J Comput Assist Tomogr*, 17(6):952–960, 1993.

25. C. R. Maurer, G. B. Aboutanos, B. M. Dawant, R. J. Maciunas, and J. M. Fitzpatrick. Registration of 3-D images using weighted geometrical features. *IEEE Trans Med Imag*, 15(6):836–849, 1996.
26. C. R. Maurer, R. J. Maciunas, and J. M. Fitzpatrick. Registration of head CT images to physical space using a weighted combination of points and surfaces. *IEEE Trans Med Imag*, 17(5):753–761, 1998.
27. D. N. Metaxas. *Physics-Based Deformable Models: Applications to Computer Vision, Graphics, and Medical Imaging*. Kluwer Academic Press, Boston, 1997.
28. C. F. Mountain. Revisions in the international system for staging lung cancer. *Chest*, 111(6):1710–1717, June 1997.
29. D. P. Naidich. Helical computer tomography of the thorax. *Radiol Clin North Am*, 32(4):759–774, 1994.
30. C. A. Pelizzari, G. T. Chen, D. R. Spelbring, R. R. Weichselbaum, and C. T. Chen. Accurate three-dimensional registration of CT, PET and/or MR images of the brain. *J Comput Assist Tomogr*, 13:20–26, 1989.
31. G. P. Penney, J. Weese, J. A. Little, P. Desmedt, D. L. G. Hill, and D. J. Hawkes. A comparison of similarity measures for use in 2-D–3-D medical image registration. *IEEE Trans Med Imag*, 17(4):586–595, August 1998.
32. U. Pietrzyk, K. Herholz, G. Fink, A. Jacobs, R. Mielke, I. Slansky, M. Würker, and W.-D. Heiss. An interactive technique for three-dimensional image registration: Validation for PET, SPECT, MR, and CT brain studies. *J Nucl Med*, 34(12):2011–2018, December 1994.
33. J. P. W. Pluim, J. B. A. Maintz, and M. A Viergever. Image registration by maximization of combined mutual information and gradient information. *IEEE Trans Med Imag*, 19(8):809–814, 2000.
34. A. H. Robinson, N. Bird, N. Screaton, E. P. Wraight, and B. F. Meggitt. Coregistration imaging the foot. a new localisation technique. *J Bone Joint Surg Br*, 80:777–780, 1998.
35. J.-M. Rouet, J. J. Jacq, and C. Roux. Genetic algorithms for a robust 3-D MR-CT registration. *IEEE Trans Inf Technol Biomed*, 4(2):126–136, June 2000.
36. D. Rueckert, L. I. Sonoda, C. Hayes, D. L. G. Hill, M. O. Leach, and D. J. Hawkes. Nonrigid registration using free-form deformations: Application to breast MR images. *IEEE Trans Med Imag*, 18(8):712–721, 1999.
37. T. G. Turkington, R. J. Jaszczak, C. A. Pelizzari, and al. Accuracy of registration of PET, SPECT and MR images of a brain phantom. *J Nucl Med*, 34:1587–1594, 1993.
38. H. Uematsu, N. Sadato, Y. Yonekura, T. Tsuchida, S. Nakamura, K. Sugimoto, A. Waki, K. Yamamoto, N. Hayashi, and Y. Ishii. Coregistration of FDG PET and MRI of the head and neck using normal distribution of FDG. *J Nucl Med*, 39:2121–2127, 1998.
39. P. A. Van den Elsen, J. B. A. Maintz, E.-J. D. Pol, and M. A. Viergever. Automatic registration of CT and MR brain images using correlation of geometrical features. *IEEE Trans Med Imag*, 14(2):384–396, 1995.
40. P. A. Van den Elsen, E.-J. D. Pol, and M. A. Viergever. Medical image matching – A review with classification. *IEEE Eng Med Biol Mag*, pages 26–39, March 1993.
41. P. Viola and W. M. Wells. Alignment by maximization of mutual information. *Int J Comput Vis*, 24(2):137–154, 1997.
42. J. B. Weaver, D. M. Healy, S. Periaswamy, and P. J. Kostelec. Elastic image registration using correlations. *J Digital Imag*, 11(3, Suppl 1):59–65, August 1998.
43. R. P. Woods, J. C. Mazziotta, and S. R. Cherry. MRI-PET registration with automated algorithm. *J Comp Assist Tomogr*, 17(4):536–546, 1993.

44. D. F. Yankelevitz and C. I. Henschke. Small solitary pulmonary nodules. *Radiol Clin North Am*, 38(3):471–478, 2000.
45. J. N. Yu, F. H. Rahey, H. D. Gage, C. G. Eades B. A. Harkness, C. A. Pelizzari, and J. W. Keyes Jr. Intermodality, retrospective image registration in the thorax. *J Nucl Med*, 36(12):2333–2338, 1995.
46. W. Zhao, T. Y. Young, and M. D. Ginsberg. Registration and three-dimensional reconstruction of autoradiographic images by the disparity analysis method. *IEEE Trans Med Imag*, 12(4):782–791, 1993.